

All-atom simulation on molecular orientation in vapor-deposited organic light-emitting diodes

Yong Youn,^{a,†} Dongsun Yoo,^{a,‡} Hochul Song,^a Youngho Kang,^a Kye Yeop Kim,^a Sang Ho Jeon,^b Youngmi Cho,^b Kyungchan Chae^b and Seungwu Han^{a*}

^aDepartment of Materials Science and Engineering and Research Institute of Advanced Materials, Seoul National University, Seoul 08826, Korea. E-mail: hansw@snu.ac.kr

^bDisplay R&D Center, Samsung Display Co., Ltd, 1 Samsung-ro, Giheung-gu, Yongin-si, Gyeonggi-do 17113, Korea.

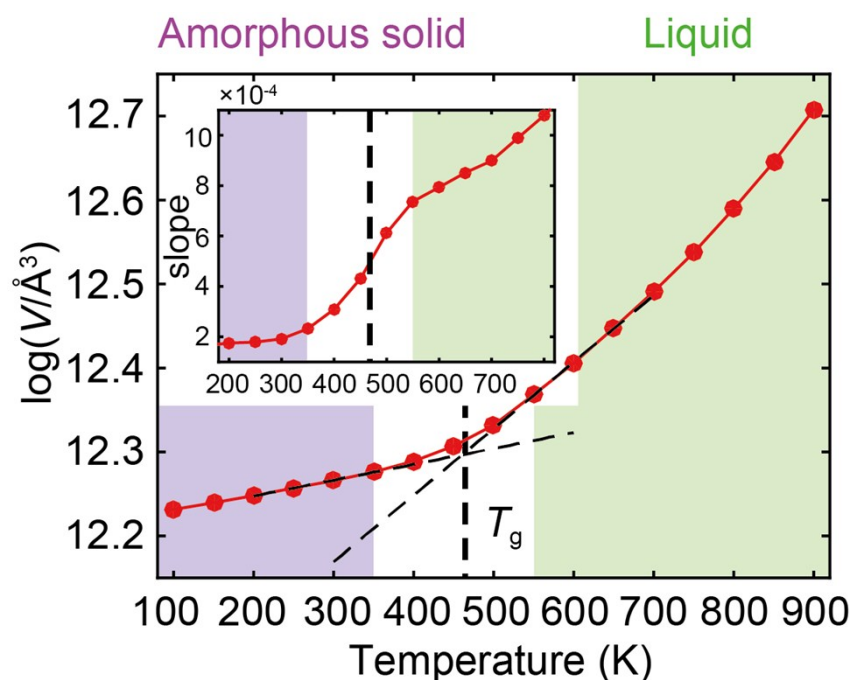


Fig. S1 Specific volume vs. temperature of CBP. The inset shows thermal expansion coefficient vs. temperature. Thin dashed lines are fitted lines and the thick dashed line indicates the glass transition temperature. Purple and green shades indicate the amorphous solid and liquid state region, respectively. Since there is an abrupt change in a thermal expansion coefficient during the transition, T_g can be estimated from the plot of cell volume vs. temperature.^{1,2} However, we noticed that T_g could not be determined by fitting two lines arbitrarily at the both ends because the thermal expansion coefficient of a liquid phase depends on the temperature. To overcome this difficulty, we divided three regions (amorphous solid, liquid and transition phase) from the plot of the thermal expansion coefficient vs. temperature. Then we determined T_g by fitting two lines to the data points that are close to the transition phase.

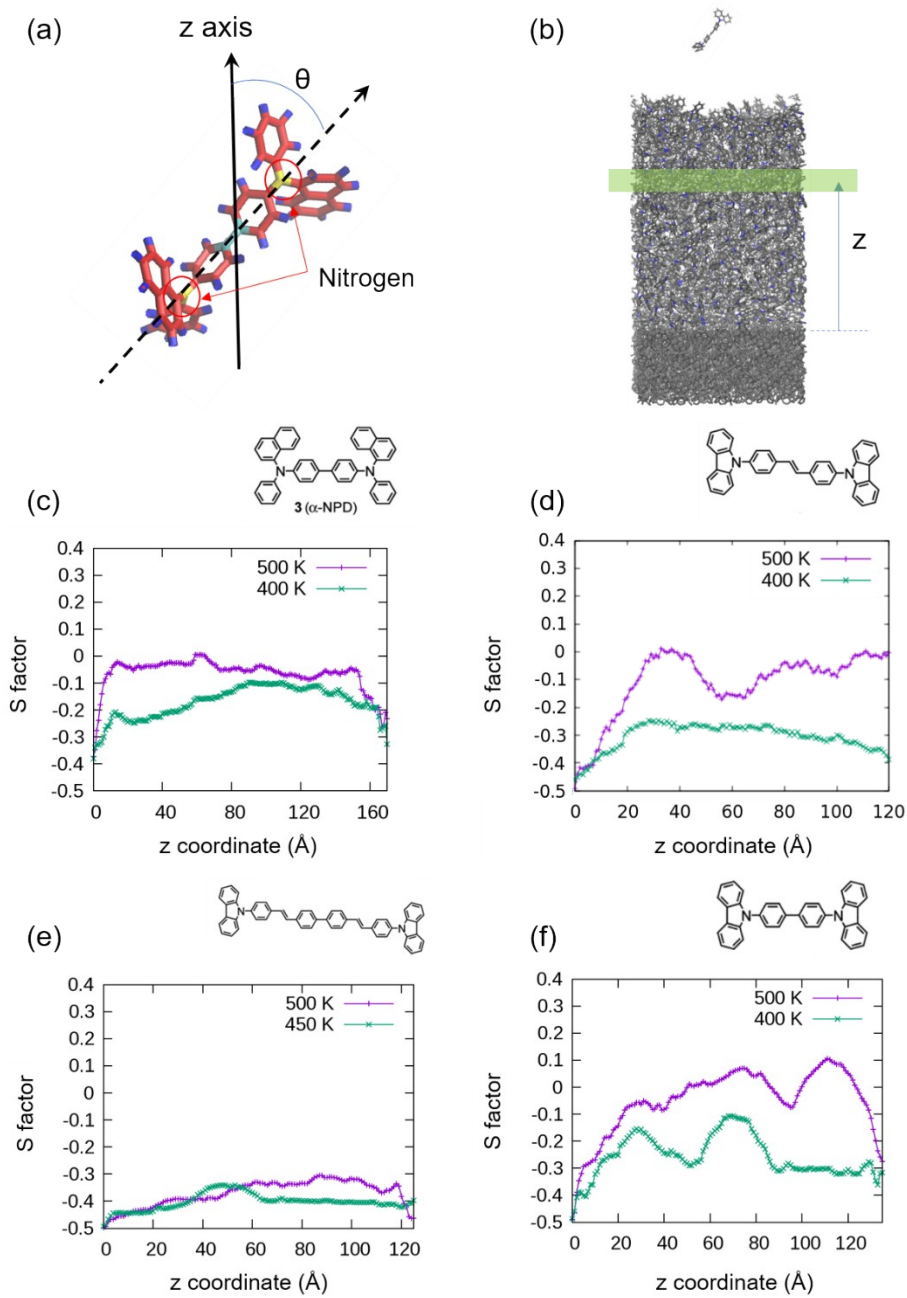


Fig. S2 Orientation order parameter S along z -axis, $S(z)$, for (c) α -NPD, (d) BCS, (e) BSB-Cz, and (f) CBP films. $S(z)$ is defined as Eq. (1) where $z(i)$ is the z -coordinate of the center-of-mass of molecule i , and $\vartheta(i)$ indicates the angle between substrate normal and transition dipole moment of molecule i . The direction of transition dipole moment is approximated by N-N direction as shown in (a). The $S(z)$ is averaged over the last 1 ns of the simulation.

$$S(z) = \frac{3}{2} \frac{\sum_i^{|z(i)-z| < \lambda} \cos^2 \theta(i)}{\sum_i^{|z(i)-z| < \lambda} 1} - \frac{1}{2} \quad \text{¥* MERGEFORMAT (1)}$$

Force field parameters

Since the conformation of α -NPD is more complex than other molecules, force field parameters of α -NPD are fitted to DFT calculations. Atomic charges are fitted from ESP charges.³ For main dihedrals, parameters are fitted to reproduce potential energy surface of constrained DFT calculations. Default OPLS-AA parameters⁴ are used for bond, angle, and Lennard-Jones interactions. For other molecules, default OPLS-AA parameters (such as biphenyl, R3N amine) are used when available. Some unavailable dihedral parameters are replaced by similar dihedral interactions. For example, dihedral parameters for CA-CA-C!-NA are replaced by those of CA-CA-C!-C!, where CA is an aromatic carbon, NA is an aromatic nitrogen, and C! is a biphenyl carbon (C! is also an aromatic carbon connected to carbazole). Parameters for carbazole are from fitted parameters of carbazole monomer.⁵ The amorphous density of CBP from MD simulation (1.13 g/cm³) is in good agreement with the experiment (1.18 g/cm³)⁶, which indicates the reliability of the parameters. Gold atoms are simply described as Lennard-Jones particles since it is not easy to integrate complex force field into OPLS-AA force field. This approach was used by Verde *et al.*⁷ The parameters from Heinz *et al.*⁸ are used to describe gold-gold interaction and the parameters from Verde *et al.*⁷ are used to describe interaction between gold and organic molecules.

Validation of force-field parameters

As mentioned above, we mainly used parameters in OPLS-AA with small modifications for BCS, CBP, and BSB-Cz. To validate these parameters, we compared them with DFT-fitted parameters by using NWChem. First, we compared default atomic charges with DFT-fitted ESP charges⁹ by plotting the electrostatic potential on the van der Waals surface (see Fig. S3). It is seen that electrostatic potential is somewhat different near the nitrogen and neighboring carbon atoms. Nevertheless, the structures of dimer conformations are similar and their relative energy ordering is the same as shown in Fig. S4. Therefore, we expect that the difference in atomic charges would not result in qualitative difference. We also compared torsional energy profile with DFT calculations (Fig. S5). The overall shape of energy profile and heights of barriers are very similar. Since the structures of BCS and BSB-Cz are similar to CBP, we concluded that default force field parameters for BCS and BSB-Cz

would be acceptable too. In conclusion, we expect that the force field parameters we used well represent the DFT calculation results.

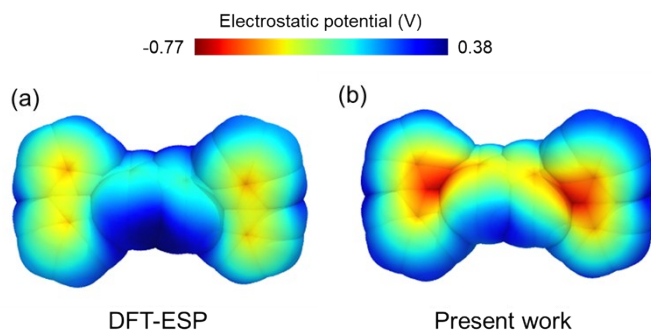


Fig. S3 The van der Waals surface of CBP molecule colored with the electrostatic potential.

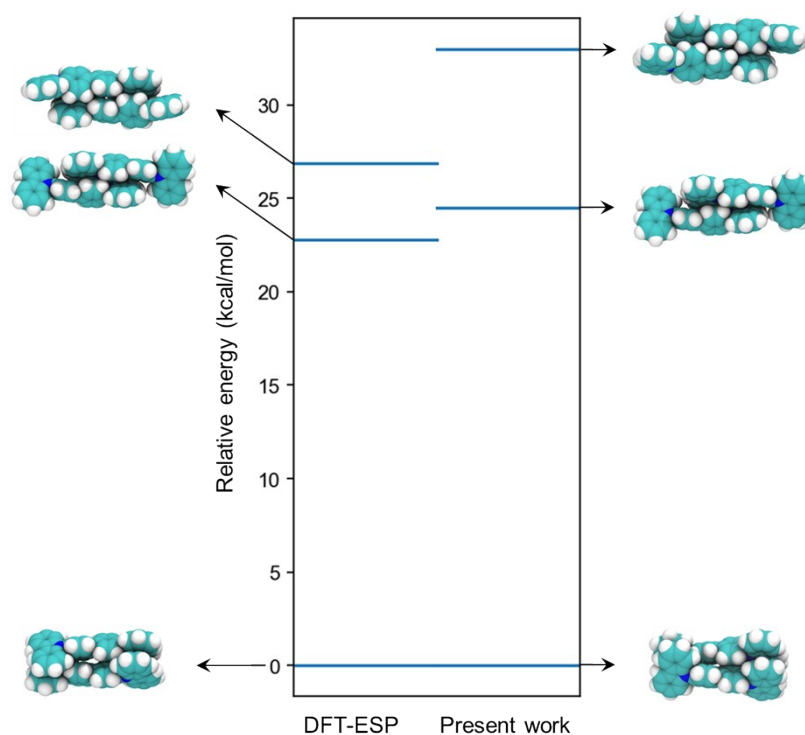


Fig. S4 Dimer conformations of CBP and their energy relative to the most stable configuration that are calculated with atomic charges from DFT-ESP or present work.

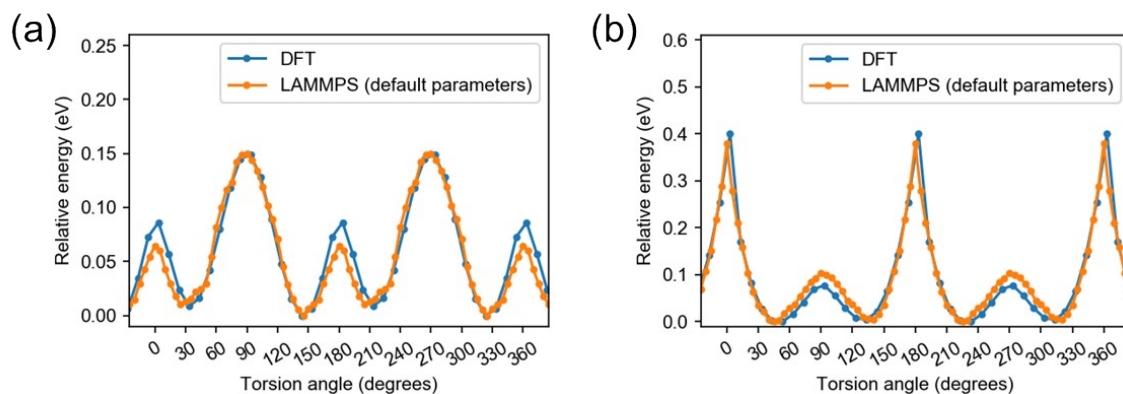


Fig. S5 The torsional energy profile of (a) biphenyl torsion and (b) torsion between biphenyl group and carbazolyl group.

Conformational energy difference

We calculated ionization potential (IP) of randomly sampled 157 molecules to examine conformational energy difference. IP is calculated with density functional theory (DFT) using NWChem software¹⁰ (PBE0 functional and 6-31g(d,p) basis set). Since the relaxation of molecule is hindered in the solid-state matrix, main torsions are fixed during the optimization. The average IP is 6.45 eV and the standard deviation is 0.041 eV. (The standard deviation of electrostatic and polarization contribution is ~ 0.11 eV.) There is almost no correlation between conformational energy difference and electrostatic/polarization energy. (Pearson correlation coefficient is 0.018.) To find out how this random disorder would affect site energy distribution, we added uncorrelated random disorder (normal distribution) of 0.041 eV to the site energy without conformational energy difference. (repeated 300 times.) The disorder over the bulk region of film increased by ~ 0.007 eV. Fig. S6 shows the influence of random disorder to the site energy correlation. Although the spatial correlation of $T_{\text{sub}} = 400$ K structure tends to decrease, it is clearly seen that the spatial correlation of $T_{\text{sub}} = 400$ K structure is still much higher than $T_{\text{sub}} = 550$ K structure. Therefore, we conclude that conformational energy difference does not affect our results and can be neglected in our system.

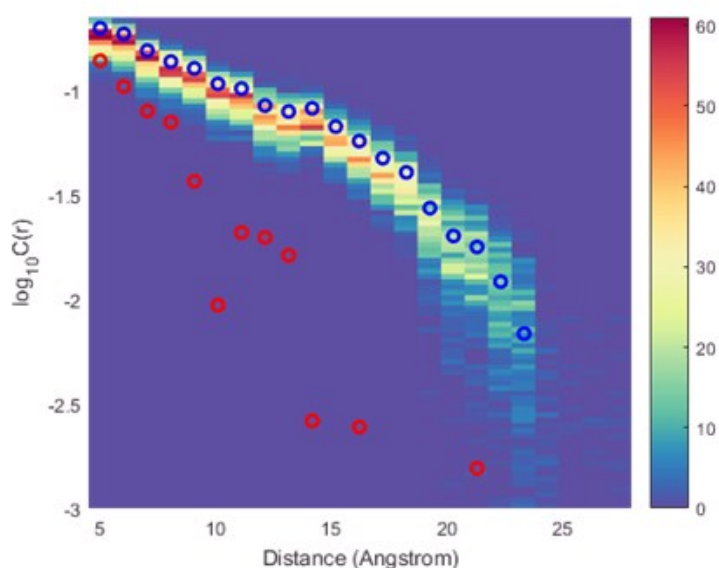


Fig. S6 Influence of uncorrelated random disorder of 0.041 eV to the site energy of $T_{\text{sub}} = 400$ K structure. Blue empty circles are $T_{\text{sub}} = 400$ K structure and red empty circles are $T_{\text{sub}} = 550$ K structure (without conformational energy difference). The color of background shows the number of occurrence of new point after adding random disorder.

Ewald summation

Since it was reported that mesoscale order can affect the energy-level profile significantly through the long-range interactions,¹¹ we use Ewald summation to include possible long-range effects originating from molecular orientation. The calculation of E 's in Eq. (2) for the charged system needs care due to the long-range nature of Coulomb force and periodic boundary conditions, which introduces spurious electrostatic interactions. Fortunately, charge correction is not required because it cancels out in Eq. (2). Slab correction (shape correction), however, needs to be considered and given in Ref. ¹². Since we are describing a periodic excitation instead of aperiodic one, there is an artifact in electric field. To minimize this, we chose the cell size that reduces the maximum error of electric field inside the film below 1 mV/Å. The error of electric field is estimated by comparing the electric field of an aperiodic point charge and the electric field of a periodic point charge on grid points (see Fig. S7). We use a 3×3×1 supercell with approximately 130-Å vacuum in the z-direction.

$$P_i = (E_{\text{solid}}^{\text{c}} - E_{\text{solid}}^{\text{n}}) - (E_{\text{gas}}^{\text{c}} - E_{\text{gas}}^{\text{n}}) \quad \text{¥* MERGEFORMAT (2)}$$

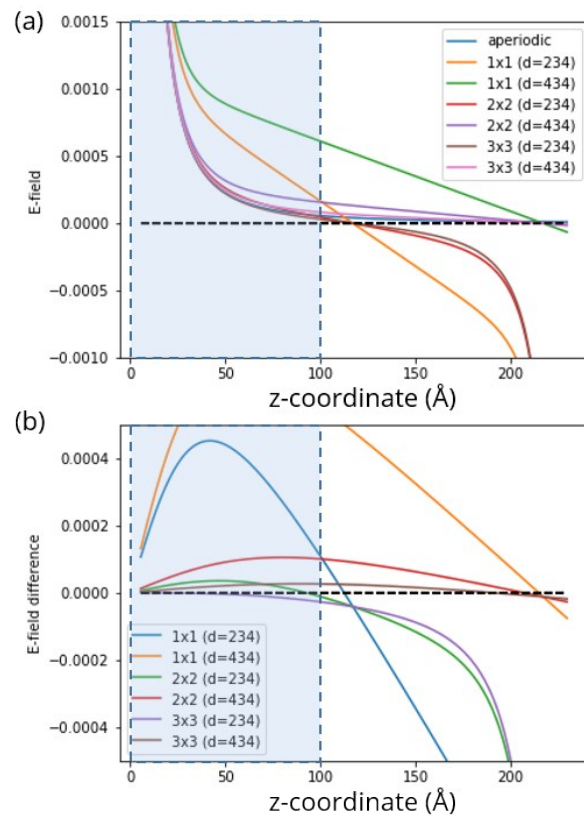


Fig. S7 (a) Electric field along z-axis and (b) electric field error along z-axis. d is the cell length in z-direction. Blue shade indicates the region where the film exists.

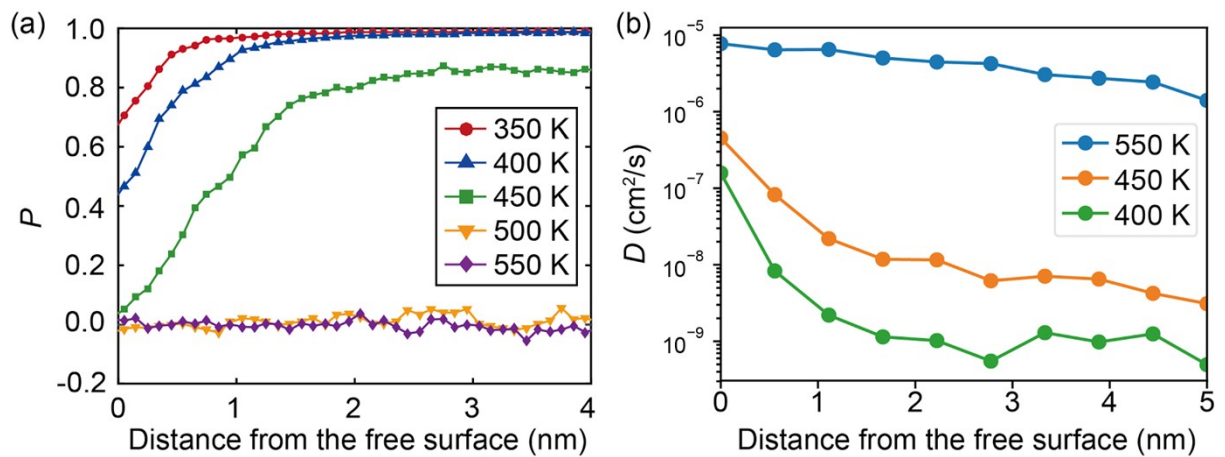


Fig. S8 (a) The change of the orientation (P) upon further deposition according to depth. P is defined as $\langle (3\cos^2\varphi - 1) / 2 \rangle$, where φ indicates an angle between the initial long molecular axis and the long molecular axis after 12.5 ns. (b) The diffusivity (D) according to the depth. The diffusivity is calculated using even sample of all available displacements for a given

duration Δt . Therefore, the number of samples is larger for smaller Δt . The P and D depending on the depth show that the mobile region is thicker at higher T_{sub} .

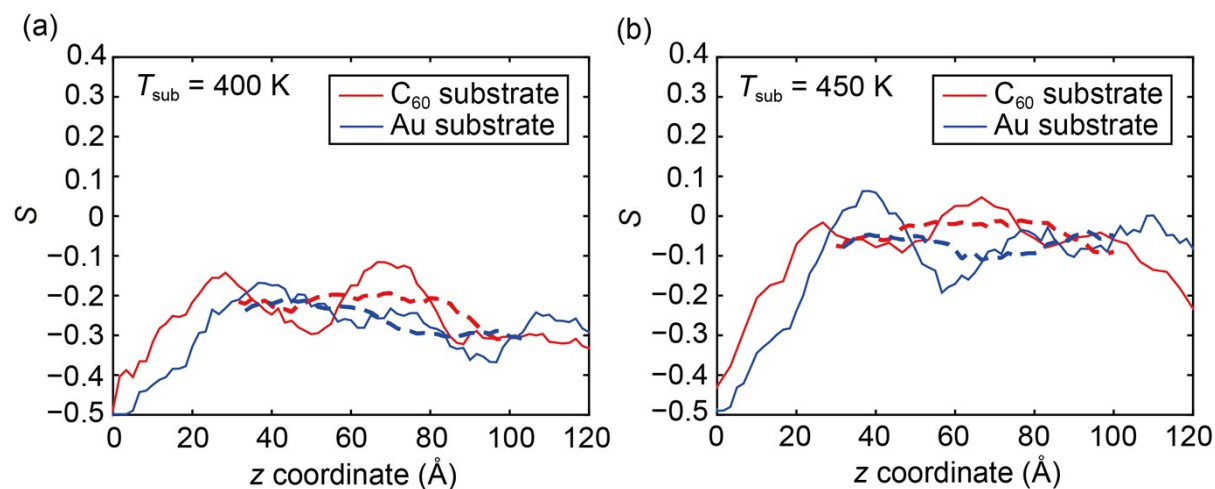


Fig. S9 Orientation order parameter S vs. z coordinate at (a) 400 K and (b) 450 K. Dashed lines indicate the orientation order parameter S within bulk region. The interface is located at $z = 0$.

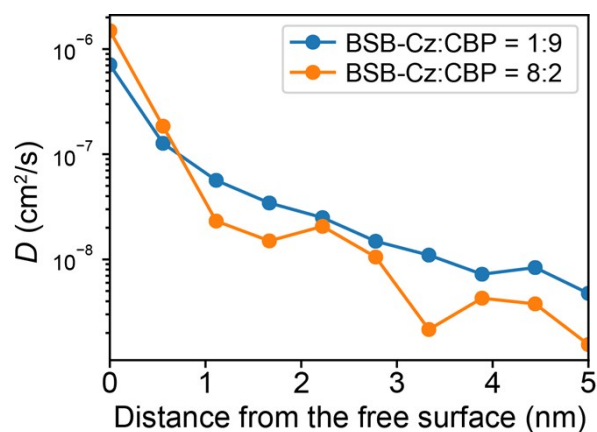


Fig. S10 The diffusivity according to the depth in a CBP/BSB-Cz mixed system. It shows that the thickness of mobile region of CBP decreases by increasing the BSB-Cz ratio because the motion of CBP dopant molecules are hindered by BSB-Cz molecules.

References

- 1 S. Kawana and R. A. L. Jones, *Phys. Rev. E*, 2001, **63**, 21501.
- 2 A. Soldara and N. Metatla, *Phys. Rev. E*, 2006, **74**, 61803.

- 3 U. C. Singh and P. A. Kollman, *J. Comput. Chem.*, 1984, **5**, 129–145.
- 4 W. L. Jorgensen, Yale University, New Haven, CT, 2009.
- 5 T. Vehoff, J. Kirkpatrick, K. Kremer and D. Andrienko, *Phys. Status Solidi Basic Res.*, 2008, **245**, 839–843.
- 6 H.-F. Xiang, Z.-X. Xu, V. A. L. Roy, C.-M. Che and P. T. Lai, *Rev. Sci. Instrum.*, 2007, **78**, 34104.
- 7 A. V. Verde, J. M. Acres and J. K. Maranas, *Biomacromolecules*, 2009, **10**, 2118–2128.
- 8 H. Heinz, R. A. Vaia, B. L. Farmer and R. R. Naik, *J. Phys. Chem. C*, 2008, **112**, 17281–17290.
- 9 C. Chipot, B. Maigret, J. L. Rivail and H. A. Scheraga, *J. Phys. Chem.*, 1992, **96**, 10276–10284.
- 10 M. Valiev, E. J. Bylaska, N. Govind, K. Kowalski, T. P. Straatsma, H. J. J. Van Dam, D. Wang, J. Nieplocha, E. Apra, T. L. Windus and W. A. de Jong, *Comput. Phys. Commun.*, 2010, **181**, 1477–1489.
- 11 C. Poelking, M. Tietze, C. Elschner, S. Olthof, D. Hertel, B. Baumeier, F. Würthner, K. Meerholz, K. Leo and D. Andrienko, *Nat. Mater.*, 2014, **14**, 434–439.
- 12 C. Poelking and D. Andrienko, *J. Chem. Theory Comput.*, 2016, **12**, 4516–4523.